Journal of Power Sources 258 (2014) 253–259

Contents lists available at ScienceDirect

Journal of Power Sources

journal homepage: www.elsevier.com/locate/jpowsour

Robustness of amorphous silicon during the initial lithiation/delithiation cycle

Lucas A. Berla [a,1], Seok Woo Lee [a,1], Ill Ryu [a,2], Yi Cui [a,b], William D. Nix [a,*]

[a] Department of Materials Science and Engineering, Stanford University, Stanford, CA 94305, USA
[b] Stanford Institute for Materials and Energy Sciences, SLAC National Accelerator Laboratory, 2575 Sand Hill Road, Menlo Park, CA 94025, USA

HIGHLIGHTS

- We probe the lithiation and delithiation behavior of amorphous silicon micropillars.
- No isolated cohesive, lithiation- or delithiation-induced pillar fracture is seen.
- Amorphous silicon is robust with respect to lithiation/delithiation.
- A diffusion-induced stress analysis supports experimental observations.

ARTICLE INFO

Article history:
Received 17 September 2013
Received in revised form
22 January 2014
Accepted 7 February 2014
Available online 21 February 2014

Keywords:
Lithium ion batteries
Lithiation
Delithiation
Amorphous silicon
Fracture

ABSTRACT

Recent research on the electrochemical lithiation of amorphous silicon nanoparticles shows that amorphous silicon is more fracture resistant than crystalline silicon during lithiation. Nanoparticles of amorphous silicon can be lithiated and delithiated without any fracture at all. To fully exploit the potential of using amorphous silicon as electrodes for lithium ion batteries it is important to determine if larger, micron-sized, amorphous silicon structures can be lithiated and delithiated without fracture. Here we study the morphologies of initially amorphous silicon micropillars (~2.3 μm tall) both before and after electrochemical lithiation and delithiation. No internal or external cohesive cracking is detected in lithiated pillars for any of the pillar sizes studied. Delithiated pillars exhibit some delamination at the interface between the pillar and the underlying nickel substrate. For larger diameter pillars, the initiated interfacial crack is driven upward into the delithiated pillar as the crack propagates radially inward. However, no cohesive fracture unrelated to interfacial cracking is seen in even the largest delithiated pillars. Finite element modeling provides support for the observation that the cohesive fracture resistance of amorphous silicon micropillars is representative of the fracture resistance of amorphous silicon microparticles of comparable dimensions.

1. Introduction

Lithium ion batteries have become the most widely used battery technology in applications requiring lightweight and high-power rechargeable energy storage [1,2]. With recent interest in electric vehicles, and accompanying the trend in increasing power consumption of rechargeable consumer electronic devices, the need for higher capacity Li-ion batteries has become a key technological issue. For the most part, commercial Li-ion battery anodes have been composed of carbonaceous material. Recently, however, silicon has received significant attention as a possible anode material, as the theoretical charging capacity of silicon is about ten times greater than that of commercialized carbon anodes [3]. Although Si offers a considerable increase in charging capacity, Si anodes suffer from large capacity fade during cycling and low cycle life. Such problem stems, in large part, from the substantial volume expansion (~300%) and contraction that Si undergoes upon Li alloying/dealloying. Due to the large volume changes, lithiation and delithiation are mechanically powerful processes that produce large stresses in Si anodes. The noted poor characteristics of Si anodes arise because such stresses give rise to anode failure, which can occur by cohesive rupture and delamination, among other mechanisms.

* Corresponding author. 496 Lomita Mall, Durand Building, Rm. 117, Stanford University, Stanford, CA 94305-2205, USA. Tel.: +1 650 725 2605; fax: +1 650 725 4034.
E-mail address: nix@stanford.edu (W.D. Nix).
[1] Equal contributions.
[2] Present address: School of Engineering, Brown University, 740 Barus and Holley, 182 Hope Street, Providence, RI 02912, USA.

http://dx.doi.org/10.1016/j.jpowsour.2014.02.032
0378-7753/

Shortcomings of Si anodes in Li-ion batteries have been ameliorated by utilizing nanostructured Si anodes, as nanostructures are much more robust with respect to fracture than bulk material [4–8]. Great progress in nanostructure synthesis, particularly in preparation of crystalline Si (c-Si) nanostructures, has enabled researchers to probe the lithiation and delithiation behavior of anodes comprised of various c-Si geometries, including pillars, spheres, and wires [9–13]. Though these crystalline nanostructures offer improvement in anode performance, such nanostructures are still susceptible to fracture during cycling, and thus capacity fade remains an issue. This outcome has prompted research into the mechanisms by which c-Si lithiates. It has now been widely observed that c-Si lithiates via a two-phase mechanism whereupon pure Si is consumed by reaction with Li, forming a heavily lithiated amorphous Li_xSi phase behind the path of the phase front, and a fully lithiated $Li_{15}Si_4$ phase is occasionally observed [14–16]. As indicated by the highly anisotropic volume expansion of c-Si upon lithiation, the velocity of the phase front depends strongly upon crystallographic orientation, with the <110> directions reacting most rapidly [17–19]. This behavior has been accounted for in some modeling research that has shed light onto the lithiation-induced stress states in crystalline silicon nanoparticles [20,21]. Some recent modeling supports empirical evidence for the presence of a critical size below which c-Si nanostructures do not fracture upon lithiation [21].

For some time, it has been widely recognized that the lithiation behavior of amorphous Si (a-Si) is substantially different from that of c-Si. Indeed, a-Si nanoparticles have recently been observed to be quite robust to fracture during cycling [22,23]. For example, using an in situ transmission electron microscopy (TEM) technique, McDowell et al. observed that hydrogenated a-Si nanoparticles are much more fracture resistant than c-Si nanoparticles, noting that a-Si spheres originally 870 nm in diameter did not fracture upon lithiation [22]. These authors also made the surprising observation that a-Si appears to lithiate by a quasi-two-phase mechanism and not single-phase diffusional insertion of Li. Wang et al. separately provided TEM evidence supporting two-phase lithiation of a-Si [25]. These observations provide a framework from which models describing the lithiation of a-Si can be developed.

The observation that nanoparticles do not fracture during lithiation is not altogether surprising, as one can expect that fracture by electrochemical shock might not occur for such small nanoparticles [9,11,24]. However, based on simple considerations of electrochemical shock one might expect fracture to occur for larger particles. An aim of this work is to explore the robustness of a-Si during lithiation/delithiation at larger size scales. Here, we present experimental and computational research on lithiation/delithiation of a-Si nano- and micro-pillars. We demonstrate that, during the initial lithiation/delithiation cycle, patterned a-Si is resistant to fracture even at the micron scale. Although we observe delamination at the pillar/substrate interface in some cases, there is no evidence of isolated internal or external cohesive fracture in the top portion of any of the pillars studied. In light of the findings of recent studies, we develop a new phenomenological finite element model for diffusional lithiation of a-Si that takes account of a steeper concentration profile than captured by a standard diffusional approach [22,25]. The modeling shows that plastic yielding severely limits the stresses that can be generated during electrochemical shock and even changes the sign of the stresses at different points in the lithiation/delithiation cycle relative to the expectations based on electrochemical shock of elastic particles. In particular, tensile stresses are generated at the surfaces during lithiation while compressive stresses are generated there during delithiation, the opposite of what might be expected based on the thermal shock analogy. Furthermore, the triaxial tensile stresses in the interior during delithiation are limited by yielding near the surface and evidently are insufficient to initiate fracture. The modeling results support our experimental findings and provide new insight into the lithiation/delithiation behavior of both a-Si and c-Si.

2. Experimental

2.1. Sample preparation

With an e-beam evaporation apparatus, a-Si films approximately 2.3 μm thick were deposited onto polished, nickel squares (purity >99.9%) with side length 5 mm and thickness 450 μm. The deposition recipe was confirmed by X-ray diffraction (Supplementary data Fig. S1) to produce amorphous films when utilized on silicon-coated nickel substrates. It is expected that films evaporated with this recipe, when deposited on uncoated nickel substrates, would similarly be amorphous. Following film deposition, pillars were milled into the a-Si films using an FEI Strata 235DB focused ion beam (FIB) with 30 keV gallium ions and concentric circle milling patterns. By performing final milling steps at low ion beam currents, pillar taper was minimized and Ni that had been redeposited onto the pillar sidewall was removed. The final pillar height was determined by the initial thickness of the film at the pillar location. Pillar heights varied from 2340 nm to 2380 nm for lithiation studies and from 2100 nm to 2460 nm for delithiation. In order to explore potential size effects, multiple pillars with diameters ranging from 600 nm–2930 nm for lithiation and 780 nm–5850 nm for delithiation were patterned onto each sample. Prior to lithiation, each pillar was imaged with the electron beam using the dual-beam FIB/SEM apparatus.

2.2. Electrochemical lithiation/delithiation

Following micromachining with the FIB, electrochemical half cells were constructed in an argon-filled glove box. In each half cell, an a-Si pillar sample served as the working electrode, and a polymer separator was placed between the working electrode and the Li foil counter/reference electrode. A solution of 1 M $LiPF_6$ in ethylene carbonate/diethyl carbonate (1:1; Merck) was used as the electrolyte. After the cells were hermetically sealed in pouches, they were removed from the glove box and the leads were connected to an Arbin BT2000 battery tester. The half cell containing pillars for lithiation was subjected to 10 mV vs. Li/Li^+, and the voltage was held at this value for 10 h. Samples with pillars that were to be delithiated were first lithiated for 10 h at 10 mV vs. Li/Li^+ and were then held at 2 V vs. Li/Li^+ for another ten hours. Some electrochemical testing results are shown in Supplementary data Fig. S2.

2.3. Characterization

Once lithiation or delithiation was completed, the sealed pouch cells were transferred back into the glove box, whereupon the pouches were opened and the pillar samples were extracted. The samples were gently washed in acetonitrile, mounted on a puck, and then sealed in vials. The argon-filled vials containing the lithiated or delithiated samples were carried to the FIB for observation. To minimize the time during which samples were exposed to the atmosphere, vials were kept sealed until the FIB chamber was fully vented. The samples were rapidly loaded into the chamber, and the chamber was then immediately pumped down. All pillars were imaged with the electron beam. Subsequent to imaging the external surfaces of the pillars, the pillars were sliced into cross sections with the ion beam to evaluate the interior morphology,

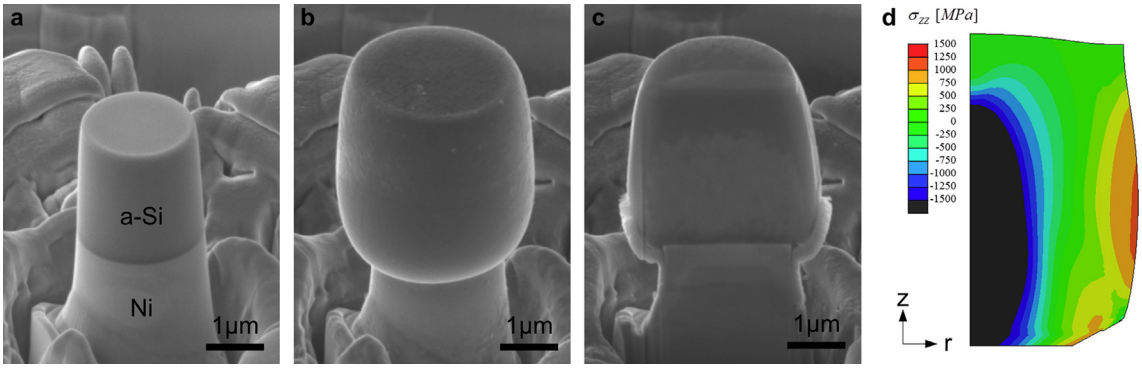

Fig. 1. Lithiation of an amorphous silicon pillar on a nickel substrate. Prior to electrochemical lithiation, the diameter and height of the pillar were 2100 nm and 2300 nm, respectively. SEM micrographs of the (a) unlithiated pillar, the (b) lithiated pillar, and a (c) FIB-milled section of the lithiated pillar are provided. No internal or external cracks can be seen. Axial stresses (σ_{zz}) predicted by simulated lithiation of a pillar are shown in (d), which illustrates half of an axial section of the fully lithiated pillar. The simulations depict large tensile (positive) stresses near the lateral surfaces (right) and compressive (negative) stresses in the interior (left).

and these cross sections were again imaged with the electron beam.

2.4. Modeling

Simulations were carried out using the ABAQUS finite element software package, and a diffusion-induced stress analysis was adopted. Seeking to capture the observation of McDowell et al. that the lithiation of a-Si appears to be a two-phase process with large concentration gradients [22], the diffusivity D of Li in Si was allowed to depend on Li fraction c through the following phenomenological form:

$$D = c^3 D_1 + (1-c)^3 D_2 \quad (1)$$

For simulated delithiation, a pillar was first lithiated with the diffusivity given by Eq. (1), and it was then delithiated using

$$D = D_1. \quad (2)$$

The parameters D_1 and D_2 were assumed to be 10^{-16} m^2 s^{-1} and 10^{-17} m^2 s^{-1}, respectively. Regardless of lithiation state, the materials parameters describing the pillar were taken to be those of lithiated Si. Specifically, the utilized pillar Young's modulus, Poisson's ratio, and yield strength were 35 GPa, 0.22, and 1 GPa, respectively. For further simplicity, the pillar was modeled as elastic-perfectly plastic, and two-dimensional axial symmetry was imposed. The transformation strain was defined so as to obtain 300% volume expansion upon full lithiation.

In all lithiation simulations, a constant concentration (fully lithiated) boundary condition was imposed at the pillar's free surfaces, although, during the first ten simulated seconds, the surface concentration was ramped from zero to this concentration. For delithiation, the surface Li concentration was decreased to zero over the course of ten seconds, and the surface concentration was then fixed at zero for the remainder of the simulation. The pillar was assumed to be fully constrained to the underlying substrate in most cases, although one simulation considered a traction-free pillar/substrate interface.

3. Results

For lithiation and delithiation studies, pillars of various diameters were milled with a focused ion beam (FIB) into evaporated a-Si films (>2 μm thick) on nickel substrates. As seen in Fig. 1, an unlithiated a-Si pillar (a), initially 2.1 μm in diameter and 2.3 μm tall, expands significantly upon lithiation (b). Though it is difficult to make an exact calculation, the volume expansion is less than but near what we would expect for a fully lithiated pillar (~300%). In Fig. 1(c), the same pillar depicted in Fig. 1(b) is sectioned in half using the FIB, with ions incident from above the pillar. Some Ni is redeposited onto the base of the lithiated Si pillar during the milling procedure, and there are minor changes in contrast on the sectioned face of the pillar possibly due to reaction of the sample with the ion beam. Neither of these artifacts, however, obscures the observation that there is no visible cohesive fracture or interfacial delamination. Fig. 1(d) shows the simulated axial stress (σ_{zz}) profile in the pillar after lithiation. The z- and θ-spatial axes are shown in the figure; this coordinate system is utilized in all simulations described in this manuscript. The rightmost surface is a lateral surface and the leftmost surface represents the central axis of the pillar simulated with this two-dimensional axially symmetric model. In the simulation, the diameter and height of the pillar prior to lithiation are taken to be 2.6 μm and 2.3 μm, respectively, and the pillar is fully constrained to the substrate at the interface. The stresses are tensile (positive) near the outer pillar surface and compressive (negative) in the interior at the end of lithiation. The hoop stresses ($\sigma_{\theta\theta}$), depicted in Supplementary data Video S1 alongside the animated axial stresses, exhibit this same trend.

Supplementary video related to this article can be found online at http://dx.doi.org/10.1016/j.jpowsour.2014.02.032.

The delithiation process is captured in Fig. 2. Fig. 2(a) depicts a pristine, unlithiated pillar with a diameter and height of 2.6 μm and 2.3 μm, respectively. This unlithiated pillar has dimensions quite similar to the one shown in Fig. 1. Fig. 2(b) illustrates clear interfacial delamination of the pillar after delithiation. However, upon inspection of the interior of the delithiated pillar via FIB sectioning—Fig. 2(c)—it is evident that the fracture is not purely interfacial. While there is delamination at the pillar/substrate interface near the outer part of the pillar, the crack turns upward and into the bulk of the pillar as it extends radially inward. The delithiation process to which this pillar was subjected is simulated using the proper diameter and height, and the pillar is again modeled as fully clamped to the underlying, rigid substrate. The resulting axial stress profile, corresponding to a moment shortly after the start of delithiation, is presented in Fig. 2(d). The axial stresses are compressive near the pillar's center and tensile close to the surfaces. Near the corner of the pillar/substrate interface there is a large tensile stress concentration where the stresses reach 1.5 GPa (dark red in the web version). Animations portraying the simulated axial and hoop stress profiles throughout the course of the lithiation/delithiation process are provided in Supplementary data Video S1. The stress profile changes during the latter stages of

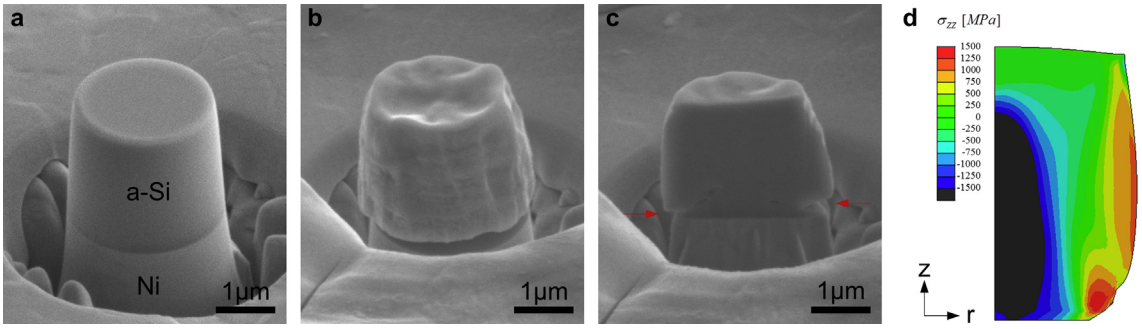

Fig. 2. Delithiation of an amorphous silicon pillar on a nickel substrate. Prior to electrochemical cycling, the diameter and height of the pillar were 2600 nm and 2300 nm, respectively. SEM micrographs of the (a) unlithiated pillar, the (b) delithiated pillar, and a (c) FIB-milled section of the delithiated pillar are provided. The delithiated pillar delaminates from the nickel near the lateral pillar surface. Tracing the adhesive crack inward, the crack turns upward and becomes a cohesive crack above the pillar/substrate interface. Axial stresses (σ_{zz}) predicted by simulated delithiation of this pillar are shown in (d), which illustrates half of an axial section of the pillar shortly after the beginning of delithiation. The simulations depict tensile (positive) stresses near the lateral surfaces (right) and compressive (negative) stresses in the interior (left). Large concentrated tensile stresses are seen near the outer corner of the pillar/substrate interface.

delithiation as tensile stresses develop in the interior and compressive stresses emerge near the lateral surfaces. Trends in the hoop stress and axial stress profiles are similar.

To understand the role of the substrate constraint on delithiation-produced delamination/cracking, we include Fig. 3, which reveals the axial stress state in a pillar at the end of delithiation predicted for different pillar/substrate interface boundary conditions. Fig. 3(a) shows the case in which the pillar is treated as being perfectly bonded to the substrate. In Fig. 3(b), the interface is assumed to be a traction-free boundary that permits free motion of the bottom surface of the Si, as shown. Both simulations were performed using the same pillar dimensions as in Fig. 2. The stresses in the bottom portion of the fully-constrained pillar—near the interface—differ significantly from those near the bottom of the traction-free pillar. However, the stress profiles in the top-half of these two simulated pillars appear notably similar. For both cases, in the top half, the stresses are mostly compressive in the outer part of the pillar and tensile in the interior. There is some obvious element distortion in simulations with a constrained interface (on the surface near the interface); however, this should not influence the stress state except very near the affected elements. Fig. 3(c), which shows an imaged section of the same pillar portrayed in Fig. 2, is included to allow side-by-side comparisons to the simulation results. All cracking is related to the initial, nucleated delamination crack. The top half of the pillar, outlined with a blue box (in the web version), is free of any visible cracks, highlighting the robustness of the upper pillar structure. We note that the compressive stresses in the outer parts of the pillar and the tensile stresses in the inner parts during the latter stages of the delithiation process are not consistent with the usual expectations based on the electrochemical shock of elastic particles. The reason is that yielding at the surface during the beginning of delithiation limits the tensile stresses that can develop there. Later in the delithiation process the removal of Li from the interior of the pillar naturally leads to tension there and compression near the surfaces of the pillar, the opposite of what is predicted based on electrochemical shock of elastic particles.

Figs. 1–3 show pillars with ~1:1 aspect ratios prior to electrochemical testing. Fig. 4 includes images of two other pillars: a pillar with a lower aspect ratio (3150 nm diameter) as well as one with a high aspect ratio (780 nm diameter). In Fig. 4, each pillar is presented in its original unlithiated state (a,d), its delithiated state (b,e), and as a FIB-milled cross section (c,f). The pillar with the high aspect ratio exhibits some delamination at the pillar sidewall (b), but cracking is not readily visible in the pillar interior (c). However, it is possible that the smallest pillars—Fig. 4(a–c)—have cohesive cracks but that these cracks are quite small and are thus concealed by material redeposited during FIB cross-sectioning. The pillar with the low aspect ratio also displays delamination on the outside (e), and upon sectioning the pillar (f) significant fracture is observed inside the pillar. The interior cracking in Fig. 4(f) resembles that of Fig. 2(c), though the fracture in Fig. 4(f) is even more apparent. Additionally, close inspection reveals that the crack in Fig. 4(f) has a small branch that propagates directly upward near the central axis

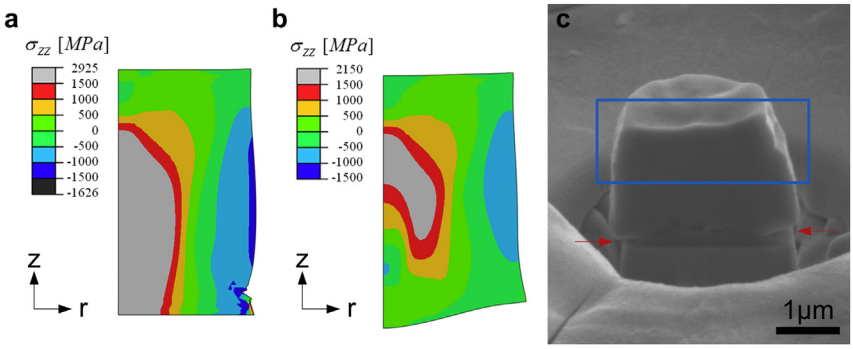

Fig. 3. The influence of boundary conditions at the pillar/substrate interface are studied. The simulated silicon pillar is assumed to be (a) fully clamped to the substrate and (b) completely free of the substrate. Both simulations describe the pillar stress state at the end of delithiation. Some insignificant element distortion appears in the bottom-right corner of the section depicted in (a). The stress profile in the top half of the pillar is similar in both cases. Included for reference is an SEM image of the simulated pillar, which has a diameter 2600 nm and height 2300 nm. The upper half of the pillar is delineated with a box, highlighting that this region is crack-free.

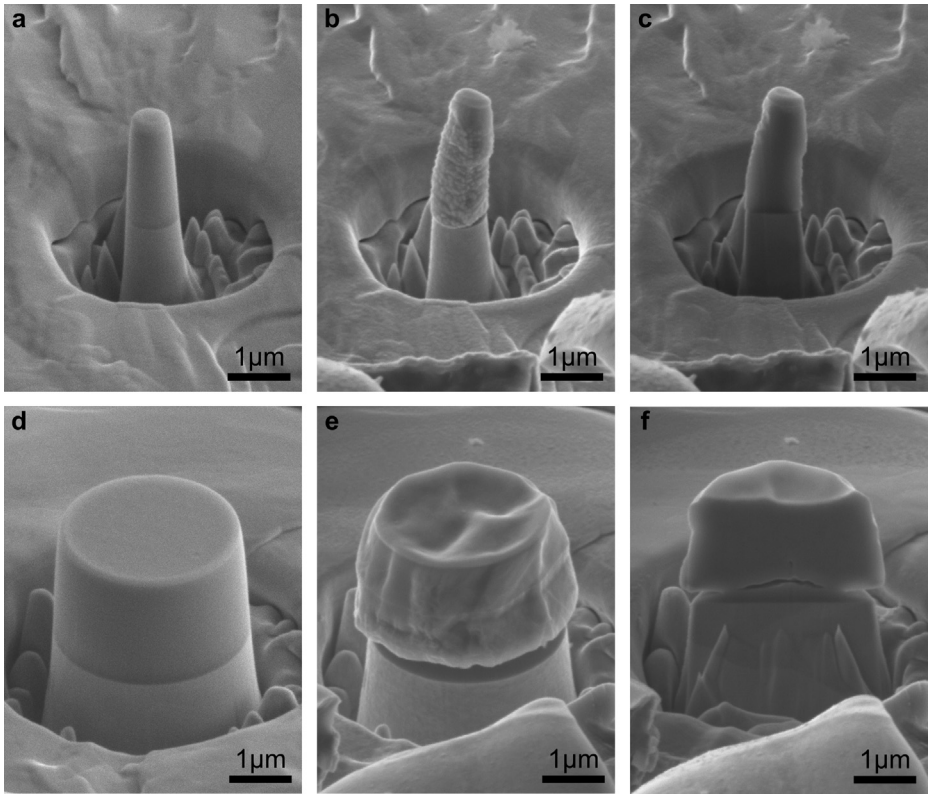

Fig. 4. Amorphous silicon pillars of other diameters are subjected to an electrochemical lithiation/delithiation cycle. A pillar with diameter 780 nm and height 2150 nm is imaged with the SEM (a) prior to lithiation, (b) following delithiation, and (c) subsequent to FIB cross-sectioning the delithiated structure. Another pillar with diameter 3150 nm and height 2100 nm is imaged (d) before lithiation, (e) after delithiation, and (f) subsequent to cross-sectioning the delithiated structure. Both pillars delaminate from the nickel substrate near the lateral surface. Interior cohesive fracture, connected to the original delamination crack, is pronounced in the wider pillar, with the crack branching near the central pillar axis and extending directly upwards. Fracture inside the smaller pillar, however, is not readily apparent.

of the pillar. Micrographs of these pillars after lithiation are not presented here, as no cracks can be detected and no remarkable observations can be made. Inspection of lithiated pillars provides evidence for occasional plastic deformation of the nickel pedestal supporting the pillars. Such deformation is speculated to have occurred during construction of the electrochemical half-cells, when pressure is applied to create contact between the components of the half-cell. The silicon pillars are not deformed or fractured during the process.

Finally, we note that one puck with a very large initial diameter (6500 nm) and relatively small height (1840 nm) was imaged after lithiation. This puck, unlike all other pillars (diameters: 600 nm–2930 nm), shows some delamination at the interface (Supplementary data Fig. S3). The delamination, which can only be seen if the pillar is sectioned, does not propagate up into the Li–Si.

4. Discussion

That lithiation does not produce cohesive fracture in any of the imaged pillars indicates that a-Si is relatively robust to the lithiation process. One measure of the robustness of a material to lithiation is its critical size—the size below which the structures do not fracture upon lithiation. Since the investigated a-Si pillars lithiate by inward diffusion of Li from all free surfaces, the critical size is defined as the smaller dimension (diameter vs. height) of the largest un-fractured pillar. Thus, the results of this work suggest that the critical size of a-Si pillars during lithiation must be larger than about 2.3 μm. By comparison, c-Si shows a critical size for lithiation-induced fracture on the order of only ~300 nm [9]. It is worth noting that large-diameter pucks may be useful for studying lithiation-induced interfacial separation, as described by others [26,27]. However, lithiation-induced delamination, though confirmed with one very wide puck (Supplementary data Fig. S3), falls outside the scope of this manuscript.

For some time, the fragility of c-Si upon lithiation has been thought to stem from both the sharpness of the phase front and from the stress concentrations that develop due to structural anisotropy [15]. Modeling provides insight relevant to this perception. The model in this work has been formulated so as to produce steep concentration profiles resembling those of a quasi-two-phase mechanism for a-Si lithiation [22]. Though not included in this manuscript, we have performed other particle lithiation simulations using an isotropic two-phase (discrete boundary) model. Additionally, we have simulated lithiation using a diffusional model with a constant, concentration-independent diffusivity. The concentration profiles differ in these two cases—steep at the boundary for the two-phase model and broad for the constant diffusivity model—yet both models, along with the concentration-dependent diffusion model represented by Eq. (1), predict hoop stresses equal to the tensile yield stress at the particle surface during lithiation. This same behavior was predicted by Zhao et al., who developed an analytical model for the stresses that evolve during isotropic two-phase lithiation of a spherical particle [20]. These four isotropic models reveal that the steepness of the concentration profile does not significantly influence the stresses responsible for particle fracture (surface stresses). For isotropic lithiation, the behavior at the surfaces is dominated by plastic yielding. On the other hand, two-phase lithiation simulations that

consider anisotropy, such as those of Ryu et al., show concentrated tensile stresses near the surfaces that exceed the yield stress [21]. With these simulation results in mind, it seems that the fragility of c-Si, at least relative to a-Si, arises chiefly from the presence of anisotropy-induced stress concentrations and not from the sharpness of the reaction front. Indeed, this is consistent with the observation of Liang et al. that crystalline germanium particles, which lithiate by a fairly isotropic two-phase mechanism, are much more robust than c-Si [28].

The simulations presented here, all of which consider diffusional transport of Li atoms in a-Si, show that the lithiation of a-Si produces tensile stresses near the pillar sidewall and compressive stresses in the interior. As noted above, this stands in sharp contrast to prior simulations of diffusion-controlled lithiation, wherein the results show compression on the outside and tension near the center [29]. The source of this critical difference is the incorporation of plasticity into the modeling. It is now evident that purely elastic simulations will produce tension in the core and compression near the surfaces during lithiation, whereas simulations that allow for plasticity will predict the inverse. Implementing plasticity, in fact, will even have this effect on simulations with some non-diffusional lithiation mechanisms, such as those involving the two-phase discrete boundary model.

Delithiation promotes delamination of the pillar from the substrate more strongly than does lithiation. Figs. 2 and 4 show that delithiation causes even high-aspect-ratio pillars to delaminate from the Ni substrate near the pillar's lateral surface. Li extraction, of course, is a process involving a large volume contraction. Hence, one might anticipate that a structure with one surface constrained to a rigid substrate, when initially subject to delithiation, will develop large tensile stresses at the interface near the structure's lateral surfaces. The constraint could produce a stress state with component stresses that exceed the interfacial adhesion strength and perhaps the tensile strength of the delithiated material. The delithiation simulations—Fig. 2(d)—predict that large σ_{zz} tensile stresses (exceeding the yield strength) are present at the interface near the sidewall shortly after delithiation commences. Such stresses would give rise to delamination at the corner of the interface, as has been observed in all delithiation experiments in this work.

The cohesive fracture observed in the interior of delithiated pillars, above the bottom interface, is not believed to indicate a general critical size for failure of Li–Si during delithiation. Instead, we argue that the substrate constraint causes interfacial delamination at the corner, and the initiated interfacial crack is driven up into the pillar, with the mixed-mode behavior potentially arising from the large stiffness of the Ni substrate relative to that of a-Si and lithiated Si. As delithiation progresses (Supplementary data Video S1) and the large, concentrated tensile stresses move inward from the lateral surfaces (and slightly upward), the initiated crack—now cohesive at its tip—continues to propagate inward (and upward). By this pathway the presence of a constraining substrate could give rise to cohesive cracks such as those observed in the pillar interiors. The constraining substrate acts as a crack initiator during delithiation. Unconstrained particles should be much more resistant to the initiation of cracks.

With the role of the substrate constraint in mind, we can comment on the critical size behavior of delithiated a-Si pillars. Noting that no delithiated pillars contain cracks unrelated to the interfacial delamination, we attribute all of the observed cohesive fractures to the interfacial constraint. The critical size for delamination-independent cohesive fracture in the bulk of the pillar during delithiation is then greater than 2.3 μm (particle size before lithiation), which represents the height of the tallest low-aspect-ratio (<1:1) pillar that was tested. Until now, very little effort has been devoted to investigating the critical size of Si during delithiation. It was only known that a-Si spheres up to 400 nm in diameter would not fracture after lithiation and subsequent delithiation [22]. We have now shown that much larger pillars can undergo lithiation and then delithiation and still exhibit no cohesive fracture unconnected to the interfacial constraint. That is, lithiated Si seems to be quite robust to cohesive fracture during delithiation.

The finding that Li–Si is robust to delithiation-induced cohesive fracture may at first seem to be specific to the pillar geometry studied in this work. The results shown in Fig. 3, however, prove the observation to be much more general. Fig. 3(a) portrays the limiting case of a pillar that is fully constrained to a substrate, and Fig. 3(b) depicts the opposite limit of a traction-free interface. Experimental observations show that, during delithiation, the pillars in fact exhibit behavior somewhere between these two limiting cases; the Li–Si pillar is initially clamped to the substrate, but interfacial tractions become relieved as cracks form and grow. In view of this and because the simulated stress profile in the top half of the pillar is similar in both limits, the top-half stress state in pillars may well represent that of isolated particles during delithiation. We may thus make predictions about free-standing particles even though we have only studied partially constrained pillars. This could be rather important, as commercial Si anodes will likely consist of unconstrained Si particles dispersed in a carbon matrix. Since the critical pillar size for lithiation/delithiation in this work appears to exceed 2.3 μm, we argue that the critical size relevant for particle lithiation/delithiation will similarly exceed 2.3 μm.

5. Conclusion

We have studied the behavior of a-Si micropillars subjected to electrochemical lithiation and delithiation. Lithiated pillars display no cohesive cracking in the pillar interior or exterior. Delithiated pillars exhibit delamination at the pillar/substrate interface near the lateral pillar surface and cohesive fracture in the pillar interior, though the cohesive fracture appears to be connected to the interfacial delamination. In assessing critical sizes for fracture, we have sought to determine whether there is visible cohesive fracture in the pillar unrelated to interfacial delamination. Our results indicate that the critical size for a-Si during lithiation must be larger than 2.3 μm, and that pertinent to Si during delithiation must also exceed 2.3 μm.

A finite element model for lithiation/delithiation of a-Si pillars, using a concentration-dependent Li diffusivity and including an elastic–plastic constitutive law, has been formulated. The results of the modeling are broadly consistent with the reported experimental observations. The modeling suggests that the fragility of c-Si during lithiation is related to the anisotropy of the Li reaction and not from the sharpness of the phase boundary. Moreover, the simulations point to the influence of substrate constraints on the structural integrity of electrochemically cycled pillars; the observed failure of delithiated Si pillars is believed to occur because of stress concentrations near the interface that are associated with the interfacial constraint. In working towards improved performance of nanostructured silicon anodes, it is thus important to ensure that constraints to volume expansion/contraction are minimized. Constraint reduction could be achieved by utilizing soft, superplastic substrates, which might promote substrate plastic deformation over interfacial delamination. Alternatively, anodes could be fabricated by embedding unconstrained silicon microparticles into deformable matrices. Future research into minimizing such constraints in nanostructured silicon anodes is important.

Acknowledgments

L.A.B. and S.W.L. contributed equally to this work. L.A.B., I.R., and W.D.N. gratefully acknowledge support of the Office of Science, Office of Basic Energy Sciences, of the U.S. Department of Energy under Contract No. DE-FG02-04ER46163. S.W.L. and Y.C. acknowledge support from the U.S. Department of Energy, Office of Basic Energy Sciences, Division of Materials Sciences and Engineering under Contract No. DE-AC02-76SF00515 through the SLAC National Accelerator Laboratory LDRD project and the Assistant Secretary for Energy Efficiency and Renewable Energy, Office of Vehicle Technologies of the U.S. Department of Energy under Contract No. DE-AC02-05CH11231, Subcontract No. 6951379 under the Batteries for Advanced Transportation Technologies Program.

Appendix A. Supplementary data

Supplementary data related to this article can be found at http://dx.doi.org/10.1016/j.jpowsour.2014.02.032.

References

[1] J.M. Tarascon, M. Armand, Nature 414 (2001) 359–367.
[2] M.S. Whittingham, MRS Bull. 33 (2008) 411–419.
[3] C.J. Wen, R.A. Huggins, J. Solid State Chem. 37 (1981) 271–278.
[4] C.K. Chan, H. Peng, G. Liu, K. Mcllwrath, X.F. Zhang, R.A. Huggins, Y. Cui, Nat. Nanotechnol. 3 (2008) 31–35.
[5] A. Magasinski, P. Dixon, B. Hertzberg, A. Kvit, J. Ayala, G. Yushin, Nat. Mater. 9 (2010) 353–358.
[6] I. Kovalenko, B. Zdyrko, A. Magasinski, B. Hertzberg, Z. Milicev, R. Burtovyy, I. Luzinov, G. Yushin, Science 334 (2011) 75–79.
[7] T.H. Hwang, Y.M. Lee, B.S. Kong, J.S. Seo, J.W. Choi, Nano Lett. 12 (2012) 802–807.
[8] H. Wu, G. Chan, J.W. Choi, I. Ryu, Y. Yao, M.T. McDowell, S.W. Lee, A. Jackson, Y. Yang, L. Hu, Y. Cui, Nat. Nanotechnol. 7 (2012) 310–315.
[9] S.W. Lee, M.T. McDowell, L.A. Berla, W.D. Nix, Y. Cui, Proc. Natl. Acad. Sci. U. S. A. 109 (2012) 4080–4085.
[10] S.W. Lee, L.A. Berla, M.T. McDowell, W.D. Nix, Y. Cui, Isr. J. Chem. 52 (2012) 1118–1123.
[11] X.H. Liu, L. Zhong, S. Huang, S.X. Mao, T. Zhu, J.Y. Huang, ACS Nano 6 (2012) 1522–1531.
[12] X.H. Liu, L.Q. Zhang, L. Zhong, Y. Liu, H. Zheng, J.W. Wang, J.H. Cho, S.A. Dayeh, S.T. Picraux, J.P. Sullivan, S.X. Mao, Z.Z. Ye, J.Y. Huang, Nano Lett. 11 (2011) 2251–2258.
[13] M.T. McDowell, S.W. Lee, I. Ryu, H. Wu, W.D. Nix, J.W. Choi, Y. Cui, Nano Lett. 11 (2011) 4018–4025.
[14] J. Li, J.R. Dahn, J. Electrochem. Soc. 154 (2007) A156–A161.
[15] M.J. Chon, V.A. Sethuraman, A. McCormick, V. Srinivasan, P.R. Guduru, Phys. Rev. Lett. 107 (2011) 045503.
[16] M.T. McDowell, I. Ryu, S.W. Lee, C. Wang, W.D. Nix, Y. Cui, Adv. Mater. 24 (2012) 6034–6041.
[17] J.L. Goldman, B.R. Long, A.A. Gewirth, R.G. Nuzzo, Adv. Funct. Mater. 21 (2011) 2412–2422.
[18] S.W. Lee, M.T. McDowell, J.W. Choi, Y. Cui, Nano Lett. 11 (2011) 3034–3039.
[19] X.H. Liu, H. Zheng, L. Zhong, S. Huang, K. Karki, L.Q. Zhang, Y. Liu, A. Kushima, W.T. Liang, J.W. Wang, J.H. Cho, E. Epstein, S.A. Dayeh, S.T. Picraux, T. Zhu, J. Li, J.P. Sullivan, J. Cumings, C. Wang, S.X. Mao, Z.Z. Ye, S. Zhang, J.Y. Huang, Nano Lett. 11 (2011) 3312–3318.
[20] K. Zhao, M. Pharr, Q. Wan, W.L. Wang, E. Kaxiras, J.J. Vlassak, Z. Suo, J. Electrochem. Soc. 159 (2012) A238–A243.
[21] I. Ryu, S.W. Lee, H. Gao, Y. Cui, W.D. Nix, J. Power Sources (2014), http://dx.doi.org/10.1016/j.jpowsour.2013.12.137.
[22] M.T. McDowell, S.W. Lee, J.T. Harris, B.A. Korgel, C. Wang, W.D. Nix, Y. Cui, Nano Lett. 13 (2013) 758–764.
[23] Y. He, X. Yu, Y. Wang, H. Li, X. Huang, Adv. Mater. 23 (2011) 4938–4941.
[24] R.A. Huggins, W.D. Nix, Ionics 6 (2000) 57–63.
[25] J.W. Wang, Y. He, F. Fan, X.H. Liu, S. Xia, Y. Liu, C.T. Harris, H. Li, J.Y. Huang, S.X. Mao, T. Zhu, Nano Lett. 13 (2013) 709–715.
[26] X. Xiao, P. Liu, M.W. Verbrugge, H. Haftbaradaran, H. Gao, J. Power Sources 196 (2011) 1409–1416.
[27] H. Haftbaradaran, X. Xiao, M.W. Verbrugge, H. Gao, J. Power Sources 206 (2012) 357–366.
[28] W. Liang, H. Yang, F. Fan, Y. Liu, X.H. Liu, J.Y. Huang, T. Zhu, S. Zhang, ACS Nano 7 (2013) 3427–3433.
[29] I. Ryu, J.W. Choi, Y. Cui, W.D. Nix, J. Mech. Phys. Solids 59 (2011) 1717–1730.